Improving fast aspheric convex surface tests with dynamic null screens using LCDs

Manuel Campos-García,[1,*] Víctor Iván Moreno-Oliva,[2] Rufino Díaz-Uribe,[1] Fermín Granados-Agustín,[3] and Agustín Santiago-Alvarado[4]

[1]Centro de Ciencias Aplicadas y Desarrollo Tecnológico, Universidad Nacional Autónoma de México, Apartado Postal 70-186, Mexico 04510, D.F. Mexico

[2]Universidad del Istmo, Ciudad Universitaria S/N, C.P. 70760, Tehuantepec, Oaxaca, Mexico

[3]Instituto Nacional de Astrofísica Óptica y Electrónica, Apartado Postal 51 and 216, 72000 Puebla, Puebla, Mexico

[4]División de Estudios de Posgrado, Universidad Tecnológica de la Mixteca, Carretera Acatlima Km 2.5, C.P. 69000, Huajuapan de León, Oaxaca, Mexico

*Corresponding author: manuel.campos@ccadet.unam.mx

Received 22 December 2010; revised 22 March 2011; accepted 28 March 2011; posted 31 March 2011 (Doc. ID 139832); published 21 June 2011

A method for testing fast aspheric convex surfaces with dynamic null screens using LCDs is shown. A flat null screen is designed and displayed on an LCD monitor with drop-shaped spots in such a way that the image, which is formed by reflection on the test surface, becomes an exactly square array of circular spots if the surface is perfect. Any departure from this geometry is indicative of defects on the surface. Here the whole surface is tested at once. The position of the spots on the LCD can be changed in a dynamic way, to perform point-shifting of the image spots. The proposed procedure improves the dynamic point-shifting method. As has been shown previously, this process reduces the numerical error during the integration procedure, thereby improving the sensitivity of the test. The positioning accuracy for the screen spots is related to the LCD's spatial resolution. Results of the evaluation of a parabolic convex surface with $f/\# = 0.22$ are shown.

OCIS codes: 220.1250, 220.4840, 120.6650.

1. Introduction

In previous work, we developed a technique for testing fast aspherical convex and concave surfaces by using null screens [1,2]. Recent advances have been successful in testing a partially specular fast spherical convex surface made of carbon fiber reinforced with polymer by using a linear null screen [3]. We have also explored the advantages of using plane-tilted null screens to increase the sensitivity in the test of an off-axis parabolic mirror [4,5]. More recently, we tested a parabolic trough solar collector based on null screen principles [6]. As has been pointed out, the null screen method measures the surface slope, and the shape of the surface can be obtained by an integration procedure [3]. The null screen method can be used to test fast aspherics, such as fast conical surfaces, free-form fast optics, and even partially specular surfaces. Recently, a quantitative slope measuring method called the software-configurable optical test system (SCOTS) has been reported [7–9], which uses similar geometry test principles as the null screen method. The SCOTS is used to test free-form illumination optics and solar collectors. This method is based on the geometry of the fringe reflection to scan the test surface [7]. Su *et al.* argue that the accuracy of SCOTS is equivalent to interferometric methods, but the details of their method are not clearly enough stated in the references, and so we have no more insight into this method.

0003-6935/11/193101-09$15.00/0

We have used the null screen procedure to test very fast aspherics; the accuracy of the test depends on many factors, such as the size, asphericity, speed ($F/\#$), and symmetry of the test surface, the size and resolution of the CCD sensor, and the focal length of the camera lens, among other factors. For all our experiments, we can state that the accuracy of the null screen methods ranges between a few to several micrometers (2–20 μm); the dynamic range, however, goes from a few micrometers to several millimeters [1–5]. These values are useful for testing optics for larger wavelengths, such as IR or millimetric waves or visible optics with specs that are not so tight, like solar concentrators or even human corneas.

For the null screen method, however, we have developed a new technique called the point-shifting method (PSM) [10,11], in order to reduce the numerical integration error and test other regions of the surface. The PSM involves increasing the number of evaluation points along the integration path. To achieve this, we proposed the movement of the cylindrical null screen along the optical axis of the surface [10]. However, in this procedure, the image points are closer along the radial direction, whereas along the azimuthal direction, the image points remain separated. More recently, a new design of the null screen was proposed with a particular array of spots designed in such a way that only rotation of the screen is needed to increase the image spot density along both the radial and azimuthal directions [11]. However, translating or even rotating the screen is a cumbersome task and can introduce alignment errors.

In order to avoid these mechanical movements of the screen, in the present paper we propose applying the PSM using LCD monitors based on the null screen principles. In the traditional test, the design points of the cylindrical null screen are plotted on a sheet of paper with the help of a laser printer or plotter, and then the paper is inserted into a transparent acrylic cylinder. Different null screens are calculated with different spot positions and are sequentially displayed on a flat LCD screen to perform the shifting of the image spots (point-shifting) [10].

Many configurations can be used to test aspherics with null screens displayed on LCDs. In this paper, we show only a simple arrangement of LCD monitors to test a fast aspheric convex surface. In Section 2, the proposed method and the setup are described in detail; the design of the screen is presented in Section 3. In Section 4, we perform an error analysis in order to determine the accuracy of the test when we have errors in the determination of both the coordinates of the centroids of the reflected image and in the coordinates of the spots of the null screen. The test of a fast convex surface ($f/\# = 0.22$) is described in Section 5. Finally, the results and the conclusions are presented at the end of the paper (Sections 6 and 7).

2. Proposed Method

The proposed setup consists of four LCDs placed in a rectangular arrangement as shown in Fig. 1.

A layout of the testing configuration is shown in Fig. 2, where the reverse exact ray-tracing and the variables involved in the design of the flat null screen displayed on the LCD monitors are shown. Here, a ray starting at P_3 in the null screen reaches the image plane at P_1, after being reflected by the mirror at P_2. If the ray starts at the LCD 1 flat screen, $x_3 = \rho$; but at LCD 1′, $x_3 = -\rho$; similarly, $y_3 = \rho'$ for LCD 2 and $y_3 = -\rho'$ for LCD 2′. Additionally, an image-forming optical system must be used to project the virtual image on a CCD sensor. Indeed, the optical system may introduce a small amount of distortion, but this can be taken into account by calibrating the system.

3. Flat Null Screen

A. Calculation of the Points on the Screen

To determine the points on the screen belonging to a square array of spots, we performed an exact ray-tracing calculation, similar to that developed for calculating the cylindrical screens to test fast surfaces (convex or concave), the expression being quite similar; they only differ in some signs [1]. To calculate the coordinates of the points on screen $P_3 = (x_3, y_3, z_3)$ that yield a perfect square array on the CCD, we worked backwards, starting at the CCD plane (see Fig. 2). Given a point $P_1 = (x_1, y_1, -a - b)$, where $-a - b$ is the distance between the vertex V of the surface to the CCD plane. Here x_1 and y_1, are the Cartesian coordinates of a point on the CCD sensor. A ray is traced back through hole P with coordinates $(0, 0, -b)$, where b is the distance between point V to the hole aperture, as shown in Fig. 2.

The coordinates $P_2 = (x_2, y_2, z_2)$ for the point of incidence on the surface are obtained by solving the simultaneous equations

$$\frac{x_2 - x_1}{-x_1} = \frac{y_2 - y_1}{-y_1} = \frac{z_2 + a + b}{a}. \tag{1}$$

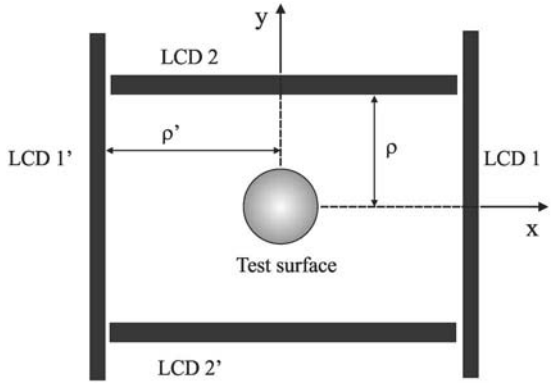

Fig. 1. Proposed schematic arrangement of the LCD monitors.

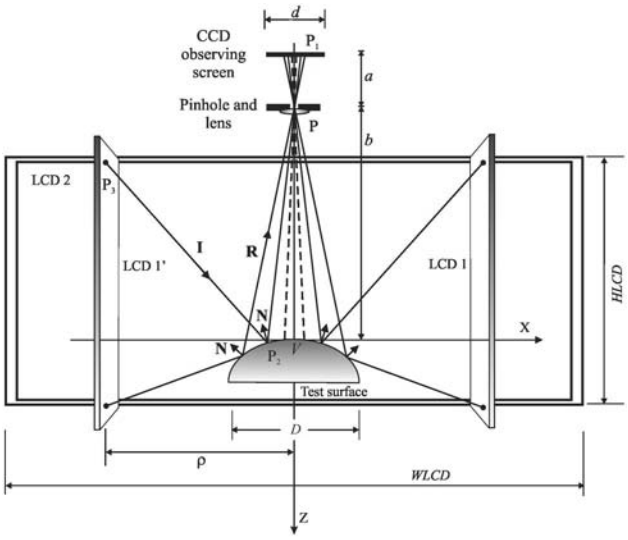

Fig. 2. Layout of the test configuration.

The reflected ray is calculated through the vector reflection law

$$\mathbf{R} = \mathbf{I} - 2(\mathbf{I}\cdot\mathbf{N})\mathbf{N} = (R_x, R_y, R_z), \tag{2}$$

where $\mathbf{I}$ is the unit incident vector given by

$$\mathbf{I} = (-x_1, -y_1, a), \tag{3}$$

and the actual normals $[\mathbf{N} = (n_x, n_y, n_z)]$ to the surface at the points P_2 are calculated from

$$\mathbf{N} = \frac{\nabla f(x,y,z)}{|\nabla f(x,y,z)|}\bigg|_{P_2}, \tag{4}$$

where

$$f(x,y,z) = Qz^2 - 2rz + x^2 + y^2 \tag{5}$$

describes a conical surface. Here r is the radius of curvature at the vertex and $Q = k + 1$ (k being the conic constant) of the test surface. Then, by substituting Eqs. (3) and (4) in Eq. (2), the components of the reflected ray are given by

$$R_x = \frac{-x_1\left[x_2^2 + y_2^2 + (Qz_2 - r)^2\right] - 2x_2\left[-x_1x_2 - y_1y_2 + a(Qz_2 - r)\right]}{x_2^2 + y_2^2 + (Qz_2 - r)^2},$$
$$R_y = \frac{-y_1\left[x_2^2 + y_2^2 + (Qz_2 - r)^2\right] - 2y_2\left[-x_1x_2 - y_1y_2 + a(Qz_2 - r)\right]}{x_2^2 + y_2^2 + (Qz_2 - r)^2},$$
$$R_z = \frac{a\left[x_2^2 + y_2^2 + (Qz_2 - r)^2\right] - 2(Qz_2 - r)\left[-x_1x_2 - y_1y_2 + a(Qz_2 - r)\right]}{x_2^2 + y_2^2 + (Qz_2 - r)^2}. \tag{6}$$

Finally, the ray hits the flat screen at P_3 with $x_3 = \rho$ for LCD 1 and $x_3 = -\rho$ for LCD 1′:

$$x_3 = \pm\rho, \qquad y_3 = \frac{R_y}{R_x}(x_3 - x_2) + y_2,$$
$$z_3 = \frac{R_z}{R_x}(x_3 - x_2) + z_2; \tag{7}$$

similarly, at $y_3 = \rho'$ for LCD 2 and $y_3 = -\rho'$ for LCD 2′,

$$y_3 = \pm\rho', \qquad x_3 = \frac{R_x}{R_y}(y_3 - y_2) + x_2,$$
$$z_3 = \frac{R_z}{R_y}(y_3 - y_2) + z_2. \tag{8}$$

Equations (7) and (8) indicate where a point, P_3, must be placed on the LCD screen to see its image at point P_1.

B. Surface Shape Evaluation

The shape of the test surface can be obtained from measurements of the positions of the incident points on the CCD plane using the formula [12]

$$z - z_0 = -\int_{p_0}^{p}\left(\frac{n_x}{n_z}\mathrm{d}x + \frac{n_y}{n_z}\mathrm{d}y\right), \tag{9}$$

where n_x, n_y, and n_z are the Cartesian components of the normal vector $\mathbf{N}$ to the test surface [Eq. (4)], and z_o is the sagitta for one point on the surface, which is not relevant, because it only yields piston error for the whole surface. This expression is exact; evaluating the normals and performing the numerical integration, however, are approximate, so they introduce some errors that must be reduced.

To evaluate the normals, $\mathbf{N}$, to the test surface, we perform a three-dimensional ray trace procedure, which consists of finding the directions of the rays that join the actual positions, P_1, of the centroids and the corresponding coordinates, P_3, of the objects of the corresponding null screen. According to the reflection law, the normal $\mathbf{N_a}$ to the test surface can be evaluated as

$$\mathbf{N_a} = \frac{\mathbf{R} - \mathbf{I}}{|\mathbf{R} - \mathbf{I}|}, \tag{10}$$

where **I** and **R** are the directions of the incident and reflected rays on the surface, respectively (see Fig. 2). In Fig. 2, the direction of the reflected ray **R** is known because after the reflection on the test surface it passes through the center of the lens stop at P and arrives at the CCD image plane at P_1, so that we have two points along this ray, which are enough to know its direction. In contrast, for the incident ray **I**, we know only the point P_3 at the null screen, so we need to have an approximate second point to obtain the direction of the incident ray; this is done by intersecting the reflected ray with a reference surface. Thus, the errors involved during the determination of the normals are minimal if the reference surface differs only slightly from the test surface [3].

Once the approximated normals to the test surface are calculated from the measurements of the centroids of the images of the null screen [Eq. (10)], the next step is the numerical evaluation of Eq. (9). A simple method used for the discrete evaluation of the integral is the trapezoidal rule for nonequally spaced data [13],

$$z_N = -\sum_{i=1}^{N-1}\left\{\left(\frac{n_{x_i}}{n_{z_i}} + \frac{n_{x_{i+1}}}{n_{z_{i+1}}}\right)\frac{(x_{i+1} - x_i)}{2} + \left(\frac{n_{y_i}}{n_{z_i}} + \frac{n_{y_{i+1}}}{n_{z_{i+1}}}\right)\frac{(y_{i+1} - y_i)}{2}\right\} + z_o, \tag{11}$$

where N is the number of points along some integration path.

C. Dynamic Point-Shifting Method

The present paper proposes an exact square arrangement of spots formed on the image plane by reflection on the test surface, if this is perfect. Each spot is designed in such a way that it has a circular shape of equal size at the CCD (0.04 mm radius); the dot shape on the screen becomes an asymmetrical oval, which we call a drop-shaped spot [14]. An initial image observed on the image plane consists of spots separated at a distance l, for a uniform sampling of the surface; after capturing the corresponding image, a new screen is designed by shifting the centers of the image points on the CCD a distance $l/2$ along the X direction (see the empty circle symbols in Fig. 3), and a second image is recorded. A third image is obtained when the screen is designed by shifting the points a distance of $l/2$ from the initial position, but now along the Y direction. Finally, a fourth image is obtained by shifting the points a distance of $l/(2)^{1/2}$ along a line 45° from the X axis, as shown in Fig. 3. Each image is processed separately to obtain the X and Y coordinates of the centroids of the spots, as is done for the static procedure [11], and all the coordinates are merged in only one ordered list to evaluate the surface with all the centroids as if all the points were included in only one screen. This gives a total of $4N$ evaluation points on the surface (N is the total number of spots in only one image); the expected average separation of the points is reduced to $l/2$.

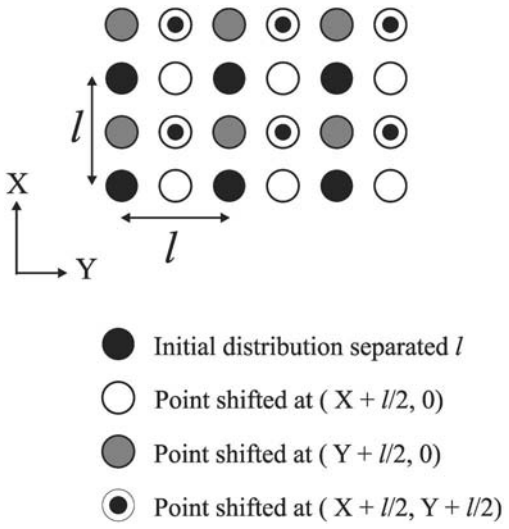

Fig. 3. Schematic representation of the PSM (image plane).

The point-shifting procedure was restricted to include only three additional points for each point on the original screen; this is not, however, a limit. More spots can be introduced with separations l/m ($m = 2, 3, 4, \ldots$) on the CCD plane. The number of images to be recorded is m^2, and the number of evaluation points along the surface is m^2N.

Figure 4 shows how the LCD null screen looks in the experimental setup. Note how the spots on the LCD screen have an almost elliptical shape, but they are oriented along different directions depending on the position. In the same way, we can observe the testing surface in front of the flat null screen.

The benefits of this point-shifting procedure were explained in [10,11]. Essentially, it is shown that the truncation error for the trapezoid integration method is reduced to ε/m, where ε, is the truncation error for a single image with N evaluation points. As has been explained, the main advantage of using the LCD monitors for displaying the null screen lies in the fact

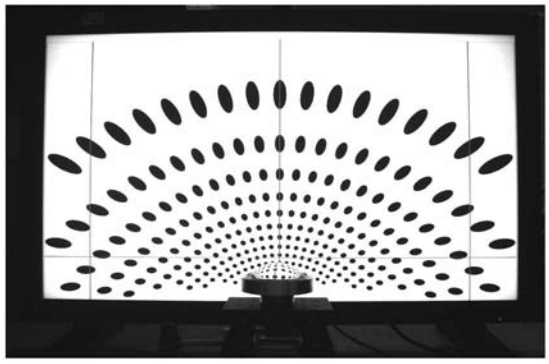

Fig. 4. LCD monitor displaying the flat null screen and test surface.

Table 1. Setup Parameters Used for the Design of the LCD Null Screen

Element	Symbol	Size
Radius of curvature	r	44.93 mm
Diameter	D	100 mm
Conic constant	k	−1
CCD–pinhole distance	a	50 mm
Stop aperture–surface vertex distance	b	729.75 mm
CCD length	d	6.6 mm
Optical axis–LCD1 distance	ρ	492.5 mm
Optical axis–LCD2 distance	ρ'	150 mm

that instead of moving the screen, as in previous papers, here nothing actually moves; the spots are only repositioned after each image is acquired. This avoids possible misalignment errors occurring during the physical movement of the screen as described in previous papers.

4. Error Analysis

In this section, we analyze the error obtained in the evaluation of the sagitta with the proposed method. In order to simulate more realistic errors, we randomly displace at the same time both the coordinates of the centroids of the bright spots on the CCD and the coordinates of the spots on the null screen [3]. We performed a numerical simulation considering an ideal surface with the same design parameters as the surface under test (see Table 1). For the simulation, we introduced random displacements in both the coordinates of the centroids on the CCD P_1, and in the coordinates of the sources (null screen objects) P_3. The random displacement functions were developed to simulate Gaussian noise [15]; they are given by

$$\delta x = \frac{\eta}{2}(-2\ln r_1)^{1/2}\cos(2\pi r_2),$$
$$\delta y = \frac{\eta}{2}(-2\ln r_1)^{1/2}\sin(2\pi r_2),$$
$$\delta z = \frac{\eta}{2}(-2\ln r_3)^{1/2}\cos(2\pi r_2), \qquad (12)$$

where r_1, r_2, and r_3 are uniformly distributed random variables that return values between 0 and 1, η is a parameter that enables control of the size of the displacement functions. For example, for $\eta = 1$ pixels, 68.4% of the values of Eq. (12) are between −0.5 and 0.5 pixels.

Then, once the displacement coordinates of the centroids are obtained, the next step is to evaluate the approximated normals $\mathbf{N_a}$ using Eq. (10). Thus, with the actual $\mathbf{N}$ [Eq. (4)] and the approximate $\mathbf{N_a}$ normals, the differences in the sagitta can be obtained in an approximate way from

$$\Delta z \approx -\int\left\{\left(\frac{n_{xa}}{n_{za}}-\frac{n_x}{n_z}\right)dx+\left(\frac{n_{ya}}{n_{za}}-\frac{n_y}{n_z}\right)dy\right\}, \qquad (13)$$

where we have assumed that $dx_a \approx dx$ (and $dy_a \approx dy$).

In Fig. 5, we show the plots of the rms differences in the sagitta Δz for different values of the parameter

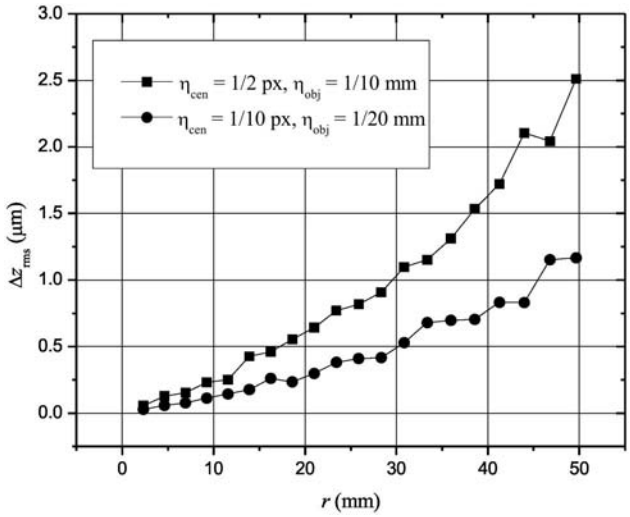

Fig. 5. Rms differences in the sagitta obtained in a simulation when a random displacement is added to the coordinates of the centroids of the spots at the CCD and to the positions of the spots of the null screen.

η against the radial coordinate of the surface. The simulation was performed considering images with 20 spots and statistics over 72 simulated images. In Fig. 5, the squares represent the differences in the sagitta for $\eta_{\text{cen}} = 0.5$ pixels and $\eta_{\text{obj}} = 0.10$ mm, and the circles represent the differences in the sagitta for $\eta_{\text{cen}} = 0.10$ pixels and $\eta_{\text{obj}} = 0.5$ mm. Here, the parameters η_{cen} and η_{obj} represent displacements in the coordinates of the centroids and of the objects, respectively. For the case of the squares, in the plot we observe that in order to have differences in sagitta smaller than 2.5 μm, the error in the measurement of the centroid coordinates must be less than 0.5 pixels, and the error in the positions of the sources of the null screen must be less than 0.1 mm. Also, if the errors in the measurements of the coordinates are less than 0.1 pixels for the positions of centroids and less than 0.05 mm for the positions of the objects of the null screen, then the error in the evaluation of the sagitta will be smaller than 1.3 μm (see the graph with circles in Fig. 5).

On the other hand, from the plots of Fig. 5, we observe that the differences in the sagitta are smaller in the center than in the rim of the test surface; this is due to the fact that the test surface is very fast.

5. Testing a Fast Convex Surface

As proof of the principle, we performed the quantitative test of a fast convex surface. In this case, the test surface is mounted on a stage that allows transversal x and y movements for easy centering, and on a lab jack to put it at the correct height position. According to [16], the test surface is a parabolic convex surface with a curvature radius of 44.93 mm, and a diameter of 100 mm ($f/\# = 0.22$). The rest of the parameters used for designing the null screen are shown in Table 1. The images were captured with a CCD camera (Sony model XC-ST70) with an active area of 8.8 mm × 6.6 mm (640 × 480 pixels), and a 16 mm

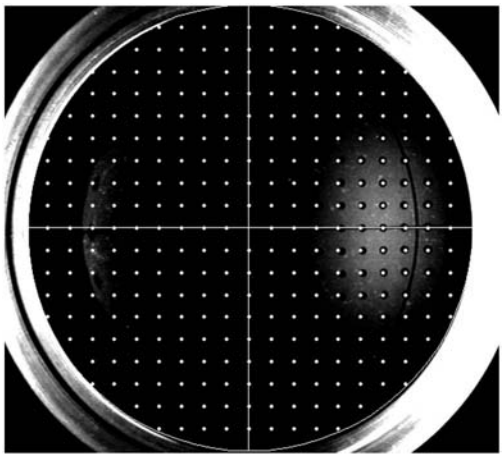

Fig. 6. Alignment of the test surface.

focal length Cosmicar TV lens attached. The lens diaphragm was used as an aperture stop. The CCD camera was located in such a position that the entire surface could be observed, so that the whole surface could be evaluated at once.

The alignment of the surface was performed manually by using a reference circle on the image of the surface with an ideal square array of spots. The circular image of the boundary of the mirror must be centered at the CCD and must touch the upper and lower boundaries of the square array of points. If this condition is not fulfilled, then the screen is misaligned or the testing surface is different from the design surface; see Fig. 6.

For the PSM, we propose four flat null screens displayed on the LCDs. According to Fig. 1, the distance between LCD 1 and LCD 1′ is proposed to be 2ρ (985 mm), and between LCD 2 and LCD 2′ it is $2\rho'$ (300 mm), both at the edge of the surface; thus, the monitors cover a greater testing area of the surface. Each of the LCD monitors is 40″ in size, with a

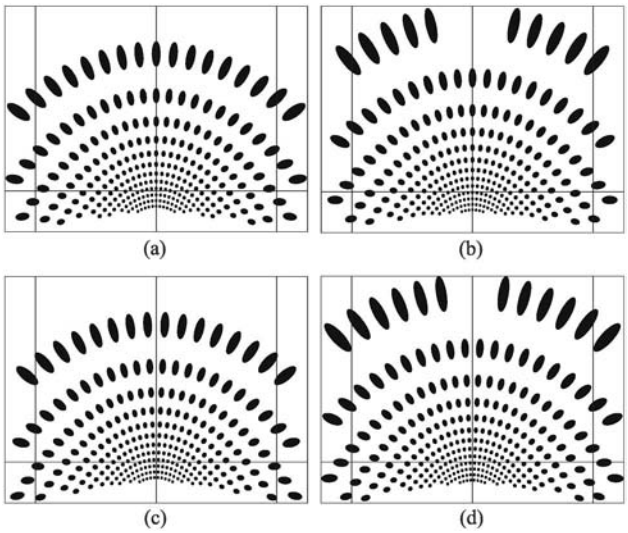

Fig. 7. Sequence of flat null screens displayed on LCD 1 and LCD 1′ to increase the number of evaluation points.

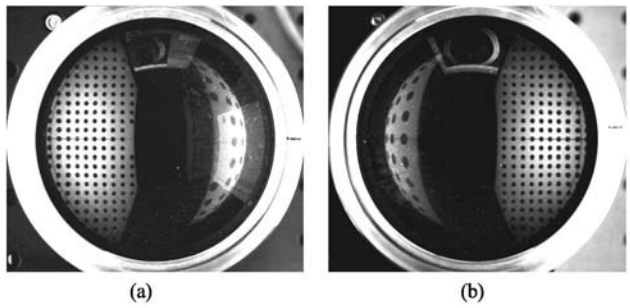

Fig. 8. First screen image of the sequence for: (a) LCD 1 and (b) LCD 1′.

resolution of 1366 × 768 pixels; the dimensions of the height (HLCD) and the width (WLCD) of the active LCDs are 885.16 mm and 497.66 mm, respectively; see Fig. 1.

To perform the dynamic point shifting, a sequence of four flat null screens is displayed on each LCD monitor. In Fig. 7, the sequence of all flat null screens for LCD 1 and LCD 1′ is shown. Figure 7(a) shows the initial null screen displayed on LCD 1 and LCD 1′; Figs. 7(b)–7(d) are the next three null screens of the sequence for the complete point shift. The image of the null screen, at the initial position of the surface, after reflection on the mirror is shown in Fig. 8. In Fig. 8(a), we show the image on the test area for LCD 1 where we observe the square array of circular spots on the left-hand side of the image, whereas on the right-hand side of the image we can observe the image of the null screen reflected on the back (second) surface of the lens. In the same way, Fig. 8(b) shows the reflected image of the flat null screen displayed on LCD 1′, where we observe the same back-reflection image. For LCD 2 and LCD 2′, the sequence of null screens for the dynamic point shifting is shown in Fig. 9. Figure 9(a) is the initial null screen displayed on the LCD monitor; Figs. 9(b)–9(d) are the next three flat screens of the sequence. Note that a smaller test area is covered for these LCD monitors; Fig. 10 shows the screen images for the initial flat screens. In order to obtain good contrast on the

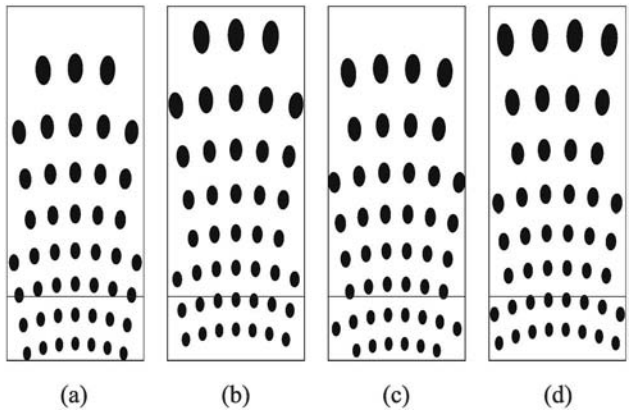

Fig. 9. Sequence of flat null screens displayed on LCD 2 and LCD 2′.

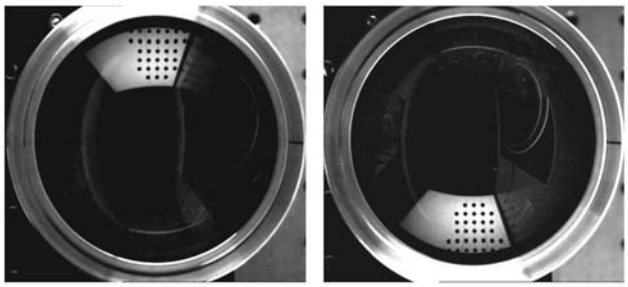

Fig. 10. First screen image of the sequence for: (a) LCD 2, and (b) LCD 2′.

images, each image is experimentally captured by switching the LCD monitors on and off, one at a time.

Four images were captured for each LCD null screen, making a total of 16 images. The centroid positions of the spots were obtained for each image with the help of ImageJ freeware [17]. All the centroids were corrected for lens distortion ($E = -5.4301 \times 10^{-9}\,\mathrm{mm}^{-2}$), and since $E < 0$, the lens presents barrel distortion. An important fact to keep in mind is that the contrast and brightness of the image depend on the angle of vision of the LCD monitor. In this configuration, the images formed by LCD 2 and LCD 2′ are brighter than those formed by LCD 1 and LCD 1′; this is probably due to the distance between the LCD monitors and the test surface. In Fig. 11, a plot of the (X, Y) coordinates of the centroids obtained with all the images is shown.

6. Experimental Results

Having collected the information on all the centroids, the approximated normals to the surface are evaluated according to the procedure proposed in Section 3.B. Then the shape of the surface is obtained

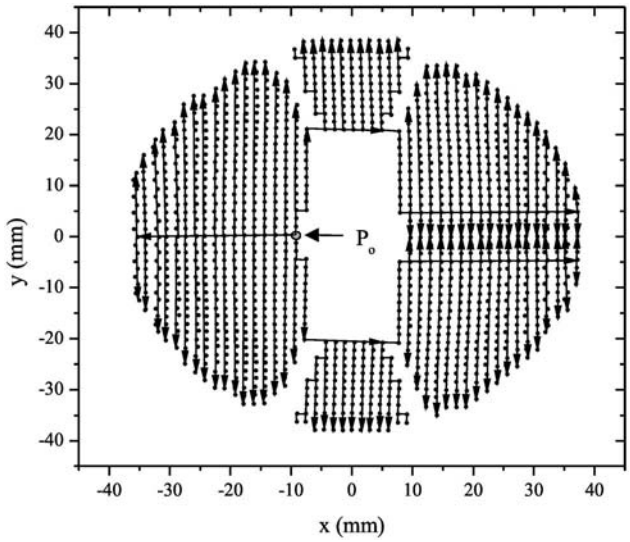

Fig. 11. Coordinates of the positions of all the centroid spots; integration paths for all the points are shown.

using Eq. (9) with the trapezoidal rule as the integration procedure [Eq. (11)]. In Fig. 11, we show the selected integration paths for all the evaluation points used for the PSM and the initial starting integration point for each trajectory, P_o; the arrowheads represent the final integration point for each trajectory. The integration paths were selected always starting at an initial point P_o. The selected paths in this configuration are simpler because the consecutive points in the path are equally spaced, along the x and y directions. Some integration paths are very large and introduce large numerical errors in the trapezoidal method used. A total of 132 paths were used for the numerical integration for all the images assembled together with the PSM. In Fig. 12, the evaluated surface is shown.

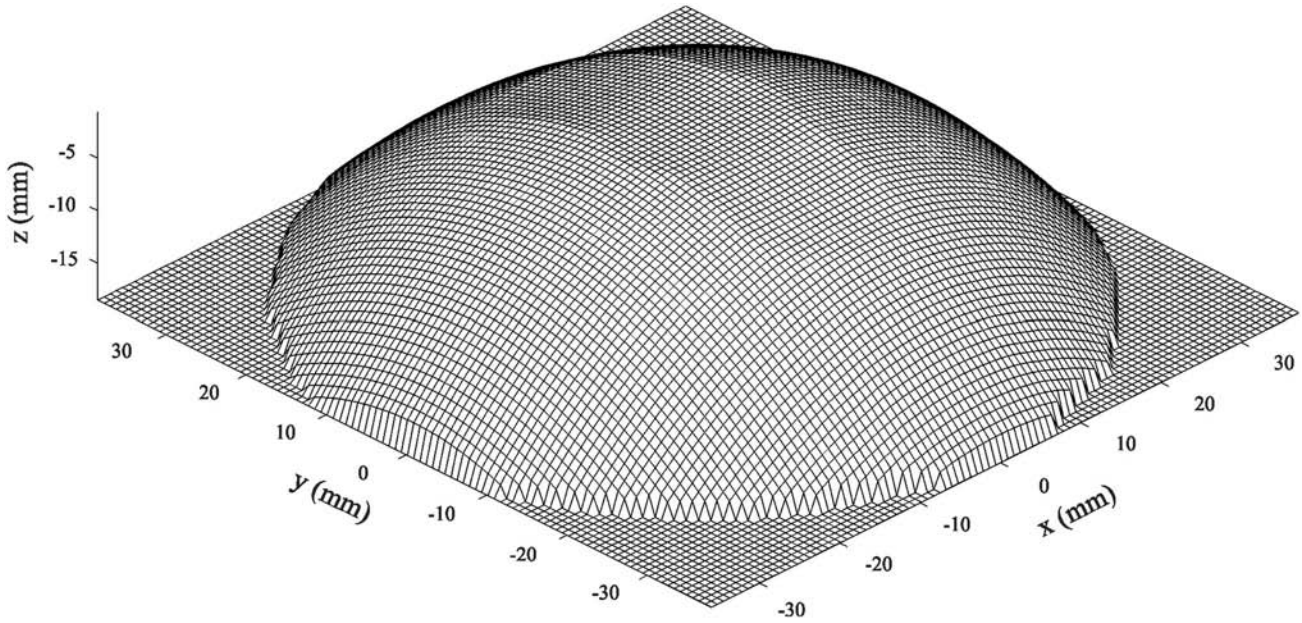

Fig. 12. Evaluated surface.

Table 2. Parameters Resulting from Least Squares Fitting of Sagitta Data: Methods

Method	r (mm)	A	B	x_o (mm)	y_o (mm)	z_o (mm)
Point-shifting LCD	42.505	0.309	0.351	−2.010	−0.002	0.001
Point-shifting radial null screen	42.259	1.995	2.297	−0.147	0.033	0.052
Laser deflectometry	43.975	-	-	-	-	-

Table 3. Parameters Resulting from Least Squares Fitting of Sagitta Data: Deformation Coefficients

Deformation Coefficients	D_1	D_2	D_3	D_4
Point-shifting LCD	-7.59×10^{-7}	1.29×10^{-9}	-6.89×10^{-13}	1.41×10^{-16}
Point-shifting radial null screen	-7.37×10^{-7}	1.34×10^{-9}	-7.72×10^{-13}	1.48×10^{-16}
Laser deflectometry	-8.22×10^{-7}	1.33×10^{-9}	-7.63×10^{-13}	1.40×10^{-16}

In order to analyze the details of the evaluation, we fit the experimental data to an aspheric surface given by

$$z = \frac{s^2}{2r} + Ax + By + D_1 s^4 + D_2 s^6 + D_3 s^8 + D_4 s^{10} + z_0, \tag{14}$$

where $s^2 = (x - x_o)^2 + (y - y_o)^2$; (x_o, y_o, z_o) are the coordinates of the vertex; (x_o, y_o) is a decentering term and z_o is a defocus; A and B are the terms of tilt in x and y, respectively; and D_1, D_2, D_3, and D_4 are the aspheric coefficients. The misalignment can be computed by fitting the experimental data to Eq. (14).

The fit to Eq. (14) was performed by using the Levenberg–Marquart method [15] for nonlinear least-squares fitting that is suitable for this task. The results of the fit are shown in Tables 2 and 3. Here we notice that the radius of curvature differs by approximately 2.43 mm or about 5.4% from other measurements ($r = 44.93$ mm) [11], but it differs by only 0.246 mm from the value obtained with the fixed null screen method.

The differences in the sagitta between the measured surface and the best fitting aspheric obtained by the least squares are shown in Fig. 13. In this case, the P-V difference in sagitta between the evaluated points and the best fit is $\delta z_{pv} = 0.072$ mm, and the rms difference in sagitta value is $\delta z_{\mathrm{rms}} = 20.8\,\mu$m.

Table 3 shows that the aspheric coefficients are very small and they are comparable to those reported in [11] with a radial null screen configuration. Here we observe that all the deformation coefficients have the same sign and order of magnitude; this result shows the repeatability of the measurements with two different null screen methods.

On the other hand, in a previous work [18], by using laser deflectometry, only one profile of the same surface was evaluated. The radius of curvature and the aspheric coefficients obtained are comparable to those obtained with the PSM (see Tables 2 and 3) showing the repeatability of the measurements with different evaluation methods.

This new null screen method allows measurement of the shape of the surface in a dynamic way. Here, departures from the perfect shape have been clearly observed. At a finer detail, the large shape variations observed in Fig. 13 are very unlikely to be real deformations of the surface. Instead, they seem to be a result of the accumulation of errors during the numerical integration procedure.

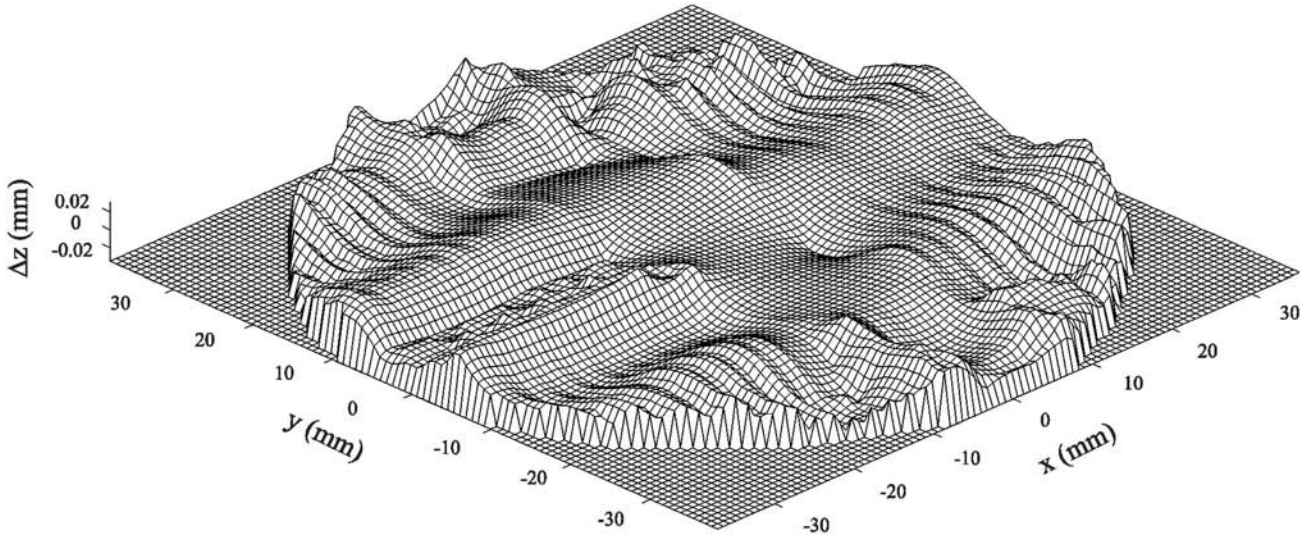

Fig. 13. Difference in the sagitta between the measured surface and the best-fitting aspheric.

7. Conclusions

We have proposed a new method for applying the PSM for testing fast convex surfaces with the null screen technique by using a configuration of four LCD monitors. In these LCDs, the flat null screens were displayed in a dynamic way, enabling us to increase the number of evaluation points and reducing the numerical error. This new procedure avoids mechanical movements of the test surface and/or the null screen.

The introduction of random displacements in the coordinates of the centroids on the CCD and in the coordinates of the sources (null screen objects) allowed us to perform an error analysis of the method. We found that in order to have differences in the sagitta smaller than 2.5 μm, the error in the measurement of the centroid coordinates must be lower than 0.5 pixels, and the error in the positioning of the sources of the null screen must be lower than 0.1 mm. An improved algorithm for obtaining a better subpixel resolution in the evaluation of the centroids of the image spots will also help to improve the accuracy of the method.

In the quantitative evaluation of the shape of the surface with the PSM, the obtained radius of curvature is less than 5.4% less than that reported in [16]. The result of the least squares fit shows that the tested surface is very close to other measurements [11,18], except for the borders, where the differences are larger because of the integration paths being longer. The fact that the results with the PSM are comparable to those obtained in previous work shows the repeatability of the test for the parabolic surface with different methods.

The result of the least squares fit shows that the tested surface has variations of approximately 20 μm rms value measure with respect to the best-fitting conic. This test, as it was implemented in the present paper, is very useful for testing very fast convex surfaces in a dynamic way and can be easily implemented, whereas the traditional test cannot be. This variant of the null screen test method is a new alternative technique for determining the quality of fast aspheric surfaces with medium accuracy. The main advantage of the test is that it is a noncontact test and does not require specially designed optics.

The authors of this paper are indebted to Neil Bruce (Centro de Ciencias Aplicadas y Desarrollo Tecnológico, Universidad Nacional Autónoma de México, Mexico) and María Fernanda Puentes-Rodriguez (Universidad Tecnológica de la Mixteca, Mexico) for revising the manuscript. This research was supported by the Consejo Nacional de Ciencia y Tecnología (CONACyT), Mexico, registered as project U51114-F, and by the Dirección General de Asuntos del Personal Académico, Universidad Nacional Autónoma de México (DGAPA-UNAM) under project Programa de Apoyo a Proyectos de Investigación e Inovación Tecnológica (PAPIIT) ES-114507.

References

1. R. Díaz-Uribe and M. Campos-García, "Null-screen testing of fast convex aspheric surfaces," Appl. Opt. **39**, 2670–2677 (2000).
2. M. Campos-García, R. Bolado-Gómez, and R. Díaz-Uribe, "Testing fast aspheric concave surfaces with a cylindrical null screen," Appl. Opt. **47**, 849–859 (2008).
3. M. Campos-García, R. Díaz-Uribe, and F. S. Granados-Agustin, "Testing fast aspheric surfaces with a linear array of sources," Appl. Opt. **43**, 6255–6264 (2004).
4. M. Avendano-Alejo and R. Dıaz-Uribe, "Testing a fast off-axis parabolic mirror using tilted null screens," Appl. Opt. **45**, 2607–2614 (2006).
5. M. Avendaño-Alejo, V. I. Moreno-Oliva, M. Campos-García, and R. Díaz-Uribe, "Quantitative evaluation of an off-axis parabolic mirror by using a tilted null screen," Appl. Opt. **48**, 1008–1015 (2009).
6. V. I. Moreno-Oliva, M. Campos-Garcia, F. Granados-Agustin, M. J. Arjona-Pérez, R. Díaz-Uribe, and M. Avendaño-Alejo, "Optical testing of a parabolic trough solar collector by a null screen with stitching," Proc. SPIE **7390**, 739012 (2009).
7. P. Su, R. E. Parks, L. Wang, R. P. Angel, and J. H. Burge, "Software configurable optical test system: a computerized reverse Hartmann test," Appl. Opt. **49**, 4404–4412 (2010).
8. P. Su, R. E. Parks, L. Wang, R. P. Angel, and J. H. Burge, "SCOTS: A quantitative slope measuring method for optical shop use," in *Optical Fabrication and Testing*, OSA Technical Digest (CD) (Optical Society of America, 2010), paper OTuB3.
9. L. Wang, P. Su, R. E. Parks, J. M. Sasian, and J. H. Burge, "Low-cost, flexible, high dynamic range test for free-form illumination optics," in *International Optical Design Conference*, OSA Technical Digest (CD) (Optical Society of America, 2010), paper ITuE3.
10. V. I. Moreno-Oliva, M. Campos-García, R. Bolado-Gómez, and R. Díaz-Uribe, "Point-shifting in the optical testing of fast aspheric concave surfaces by a cylindrical screen," Appl. Opt. **47**, 644–651 (2008).
11. V. I. Moreno-Oliva, M. Campos-García, and R. Díaz-Uribe, "Improving the quantitative testing of fast aspherics with two-dimensional point-shifting by only rotating a cylindrical null screen," J. Opt. A **10**, 104029–104035 (2008).
12. R. Díaz-Uribe, "Medium-precision null-screen testing of off-axis parabolic mirrors for segmented primary telescope optics: the large millimeter telescope," Appl. Opt. **39**, 2790–2804 (2000).
13. W. H. Press, B. P. Flannery, S. A. Teukolsky, and W. T. Vetterling, *Numerical Recipes in C: The Art of Scientific Computing* (Cambridge University, 1990).
14. L. Carmona-Paredes and R. Díaz-Uribe, "Geometric analysis of the null screens used for testing convex optical surfaces," Rev. Mex. Fís. **53**, 421–430 (2007).
15. P. R. Bevington and D. K. Robinson, *Data Reduction and Error Analysis for the Physical Sciences*, 2nd ed. (McGraw-Hill, 1992), pp. 161–166.
16. R. Díaz-Uribe and A. Cornejo-Rodríguez, "Conic constant and paraxial radius of curvature measurement for conic surfaces," Appl. Opt. **25**, 3731–3734 (1986).
17. W. Rasban, National Institutes of Health, USA. Image J V. 1.312u, *Image Processing and Analysis in Java* http://rsb.info.nih.gov/ij/.
18. M. F. González-Cardel and R. Díaz-Uribe, "Profile and deformation coefficients measurement of fast optical surfaces," Opt. Express **14**, 9917–9930 (2006).